Magnetic Nanofluids (MNFs) Radiative Flow Over a Moving Surface with Convective Boundary Condition

Nur Syahirah Wahid[1], Norihan Md Arifin[1,2(✉)], Najiyah Safwa Khashi'ie[3], Ioan Pop[4], Norfifah Bachok[1,2], and Mohd Ezad Hafidz Hafidzuddin[5]

[1] Department of Mathematics and Statistics, Faculty of Science, Universiti Putra Malaysia, UPM, Serdang, 43400 Seri Kembangan, Selangor, Malaysia
norihana@upm.edu.my
[2] Institute for Mathematical Research, Universiti Putra Malaysia, UPM, Serdang, 43400 Seri Kembangan, Selangor, Malaysia
[3] Fakulti Teknologi Kejuruteraan Mekanikal Dan Pembuatan, Universiti Teknikal Malaysia Melaka, Hang Tuah Jaya, 76100 Durian Tunggal, Melaka, Malaysia
[4] Department of Mathematics, Babeş-Bolyai University, R-400084 Cluj-Napoca, Romania
[5] Centre of Foundation Studies for Agricultural Science, Universiti Putra Malaysia, UPM, Serdang, 43400 Seri Kembangan, Selangor, Malaysia

Abstract. Magnetic nanofluids (MNFs) have recently piqued the interest of many experts because of their capability and significance in various real applications. Hence, in this study, we want to numerically highlight the influence of convective boundary conditions and radiation on the magnetic nanofluids (MNFs) flowing past a permeable moving plate. The governing flow model in partial differential equations (PDEs) is transformed into ordinary differential equations (ODEs) using suitable similarity variables. The ODEs are solved by implementing the built-in solver in Matlab called bvp4c. The relevant specification of the parameters led to the execution of two numerical outputs. We have finalized the investigation by incorporating a stability analysis to confirm the stability qualities conveyed by the outputs. The stability analysis has supported our initial presumption that only one of the outputs is stable. In this present study, the thermal performance between cobalt ferrite nanofluid and manganese-zinc ferrite nanofluid is compared, and it appears that cobalt ferrite nanofluid has a slightly better performance in heat transportation compared to manganese-zinc ferrite nanofluid. We also considered a higher amount of thermal radiation and Biot number to scrutinize the heat transfer performance of MNF. We found that the immense value of these parameters effectively improves the heat transfer rate. The skin friction coefficient is magnified when the plate moves towards the slit, but the heat transportation performance is higher when the plate moves out from the slit. This research is significant because it simulates the thermal performance of MNFs when greater radiation and convective heat are applied to a moving plate; therefore, it could be used as a guide for actual applications that involve the heat transfer process.

Keywords: Nanofluid · Thermal radiation · Moving surface · Convective boundary condition · Stability analysis

N. Wahi et al. (Eds.): ICMSS 2022, ACSR 98, pp. 67–84, 2023.
https://doi.org/10.2991/978-94-6463-014-5_8

1 Introduction

In many engineering applications, there are scenarios of continuous moving surfaces, for which an accurate estimate of the material's axial temperature fluctuation is critical. For instance, this happens during the lamination and melt-spinning processes, hot steel extrusion, aerodynamic extrusion of plastic sheets, and heat treatment for material moving between windup rolls [1, 2]. Sakiadis [3, 4] was the pioneer to research boundary layer flow due to a moving, continuous surface where he has discovered the disparity of boundary layer between a finite-length surface and a continuous moving surface. After his effort, the investigation has been followed by several researchers, including Chappidi and Gunnerson [5], Afzal [6], Howell et al. [7], Weidman et al. [8], and Ishak et al. [9] in analyzing the momentum or heat transmission for laminar/turbulent boundary layer flow past a moving surface.

Subhashini and Sumathi [10] have addressed the study on mixed convection flow over a moving vertical plate by considering copper, alumina, and titania nanofluids instead of regular classical fluid. The findings reveal the existence of dual solutions when the plate and free stream move in the same direction and the opposite direction. Later, Das and Jana [11] consider the same flow geometry but with the additional magnetic field and thermal radiation towards the flow that only concerning to natural convection. By utilizing the hybrid nanofluid, Aladdin et al. [12], Waini et al. [13], and Khashi'ie et al. [14] reported that the duality of the solution only exists when the moving parameter moves towards the negative direction such that the plate moves in the adverse direction of the free stream. Further, Anuar et al. [15] stated in their investigation that the temperature and velocity distribution of nanofluids with carbon nanotubes accelerate with increasing moving parameter. From the literature, we can see that nanofluids have merited in-depth research and investigative focus among the researchers. Recent research also shows that nanofluids perform better at heat transfer than regular fluids, and that improvement enhances when the Reynolds number and nanoparticle volume fraction increase [16, 17].

Magnetic nanofluids (MNFs) or ferrofluids, are a subclass of nanofluids that consist of colloidal suspensions of nanoscale magnetic particles (usually 5–10 nm) that show both magnetic and fluid characteristics. Magnetic nanoparticles (MNPs) for this fluid are often synthesized in a variety of sizes and shapes from metals along with their oxides such as iron oxide, cobalt ferrite, and Mn-Zn ferrite in either polar or non-polar liquid carriers such as oil, ethylene glycol and water. The primary benefit of MNFs is their ability to adjust viscosity in a short period [18]; meanwhile, the MNPs in the suspension neither form sediment in the gravitational/moderate magnetic field because of their small size nor aggregate due to the magnetic dipole interaction [19]. This kind of fluid also can minimize skin friction, and an external magnetic field can be inserted to alter the heat transmission rate and flow characteristics of the fluid [20].

In retrospect, MNF was invented at the National Aeronautics and Space Administration's (NASA) Research Center in 1963. Since that, researchers have taken an interest in MNF investigation due to the various needs in a variety of sectors. The broad applications of MNF, for example, in electronics devices, heat transfer applications, medical applications, and optical devices, have been discussed by the following authors: Raj and Moskowitz [21], Marszałł [22], Kumar and Subudhi [23], Kole and Khadekar [24]. Many

works have reported experimental studies and numerical studies regarding MNFs with different objectives and methods. For further details regarding the investigation towards nanofluids, some of the literature is listed in the following references: [25–33].

In this present study, the main purpose is to extend the numerical research on the boundary layer flow over a moving permeable surface which has been previously proposed by Weidman et al. [8]. Inspired by the emerging concept of nanofluids, we have upgraded the research by considering magnetic nanofluids which are cobalt ferrite/water nanofluid and Mn-Zn ferrite/water nanofluid. As looking through the preceding literature, cobalt ferrite and Mn-Zn ferrite are among of the magnetic nanoparticles that have been considered by many researchers; however, the numerical investigation on these fluids is still limited and should be continuously extended with various flow configurations to specifically imitate the real-life applications. Hence, for a novelty purpose, several additional parameters have been incorporated in this present study, such as thermal radiation and convective boundary condition to contemplate their effects towards the magnetic nanofluids. The heat transfer ability between these two considered magnetic nanofluids are also investigated and compared. Not just that, we also adopted the correlations of the thermophysical properties for the nanofluids that have been validated experimentally by Ho et al. [34]. The stability analysis is performed by using the procedure prescribed by Merkin [35] and Harris et al. [36] as we detected two solutions from the model. Thus, with the provided findings, we hope scientists and engineers can better forecast the features of MNFs convective flow in advanced technological systems like transportation, power production, chemical industries, and electronics.

2 Mathematical Model

Consider the two-dimensional flow and heat transfer of MNFs across a permeable moving flat plate where (x, y) are the Cartesian coordinates, that we supposed the x-axis runs along the plate and the y-axis is normal to the plate's surface, the flow being at $y \geq 0$ (see Fig. 1).

For thermal enhancement, two distinct magnetic nanoparticles (MNPs), namely $CoFe_2O_4$ (cobalt ferrite) and Mn-$ZnFe_2O_4$ (manganese-zinc ferrite) are diluted in the water-base nanofluid. The moving plate and the far-field velocities are U. The mass flux velocity is $v_w(x)$ with $v_w < 0$ for suction and $v_w > 0$ for the injection. The plate's bottom surface is heated by convection from a hot fluid at a temperature T_f with a heat transfer coefficient $h_f(x) = (2x)^{-1/2}a$, where a is a constant (see Kameswaran et al. [37]). The temperature far from the plate (inviscid base fluid) is denoted by T_∞ and the radiative heat flux q_r is imposed.

Following the described assumptions, the boundary layer equations and the boundary conditions are (see Weidman et al. [8]; Kameswaran et al. [37])

$$\frac{\partial u}{\partial x} + \frac{\partial v}{\partial y} = 0 \tag{1}$$

$$u\frac{\partial u}{\partial x} + v\frac{\partial u}{\partial y} = \frac{\mu_{nf}}{\rho_{nf}}\frac{\partial^2 u}{\partial y^2} \tag{2}$$

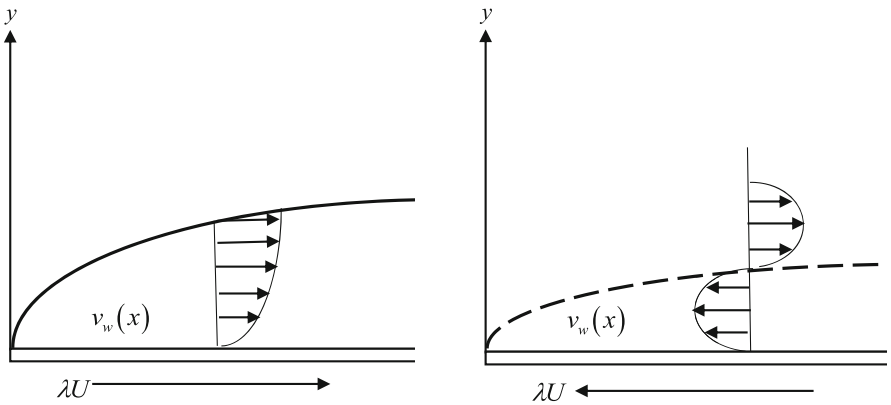

a) Moving plate out of the slit $(\lambda > 0)$ b) Moving plate towards the slit $(\lambda < 0)$

Fig. 1. Physical model and coordinate system

$$u\frac{\partial T}{\partial x} + v\frac{\partial T}{\partial y} = \frac{k_{nf}}{(\rho C_p)_{nf}}\frac{\partial^2 T}{\partial y^2} - \frac{1}{(\rho C_p)_{nf}}\frac{\partial q_r}{\partial y} \tag{3}$$

$$\left.\begin{aligned} v = v_w(x),\ u = u_w = U\lambda, \\ -k_{nf}\frac{\partial T}{\partial y} = h_f(x)(T_f - T) \end{aligned}\right\}, \text{at } y = 0, \qquad u_e \to U,\ T \to T_\infty \text{ as } y \to \infty. \tag{4}$$

Here, u and v are the velocity components along x and y axes, T is the temperature of the nanofluid and λ is the moving parameter with $\lambda > 0$ for the moving plate outside of the slit, $\lambda < 0$ for the moving of the plate toward the slit, and $\lambda = 0$ for the static plate, respectively.

Further, the correlations for the properties of MNF are given in Table 1 [34, 38], where the properties consist of the density ρ, heat capacity ρC_p, dynamic viscosity μ, and thermal conductivity k, while the value for each property is tabulated in Table 2 [39]. In these tables, ϕ is the nanoparticle volume fraction, where $\phi = 0$ corresponds to a classical viscous fluid. The subscripts of *nf, f,* and *s,* on each of the properties, denote MNF, base fluid (liquid), and MNP, respectively.

For the radiative heat flux q_r in Eq. (3), according to Rosseland approximation, we can simply express the term as follows [40–45]:

$$q_r = -\frac{4\sigma^*}{3k^*}\frac{\partial T^4}{\partial y} \tag{5}$$

Table 1. The correlation of thermophysical characteristics of MNF (see Ho et al. [34] and Sheremet et al. [38])

Properties	Correlations
Density	$\rho_{nf} = (1-\phi)\rho_f + \phi\rho_s$
Heat capacity	$(\rho C_p)_{nf} = (1-\phi)(\rho C_p)_f + \phi(\rho C_p)_s$
Dynamic viscosity	$\frac{\mu_{nf}}{\mu_f} = \frac{1}{(1-\phi)^{2.5}}$
Thermal conductivity	$\frac{k_{nf}}{k_f} = \frac{k_s+2k_f-2\phi(k_f-k_s)}{k_s+2k_f+\phi(k_f-k_s)}$

Table 2. Thermal and physical characteristics for MNF compositions (see Ahmed et al. [39])

Properties	$\rho\left(\text{kg/m}^3\right)$	C_p(J/kgK)	k(W/mK)	Pr
H_2O	997.1	4179	0.613	6.96
$CoFe_2O_4$	4907	700	3.7	–
Mn-$ZnFe_2O_4$	4900	800	5.0	–

where k^* and σ^* are the mean absorption coefficient and Stefan-Boltzmann constant, respectively. T^4 is extended about T_∞ using the Taylor series and omitting higher-order terms to obtain $T^4 \approx 4T_\infty^3 T - 3T_\infty^4$. So, Eq. (3) may thus be expressed as

$$u\frac{\partial T}{\partial x} + v\frac{\partial T}{\partial y} = \frac{1}{(\rho C_p)_{nf}}\left(k_{nf} + \frac{16\sigma^* T_\infty^3}{3k^*}\right)\frac{\partial^2 T}{\partial y^2} \tag{6}$$

To simplify the flow model, we consider the Blasius similarity transformation [8],

$$\begin{aligned} &u = Uf'(\eta),\ v = -\left(\frac{Uv_f}{2x}\right)^{1/2}\left[f(\eta) - \eta f'(\eta)\right], \\ &\theta(\eta) = \frac{T-T_\infty}{T_f-T_\infty},\ \eta = y\sqrt{\frac{U}{2xv_f}} \end{aligned} \tag{7}$$

also, the transpiration effect (suction/injection) is given as,

$$v_w(x) = -\left(\frac{Uv_f}{2x}\right)^{1/2} S \tag{8}$$

where the prime denotes differentiation to η, $v_f = \mu_f/\rho_f$ is the kinematic viscosity of the base fluid, and S is the constant mass flux velocity, with $S > 0$ for suction and $S < 0$ for injection, respectively.

Applying Eq. (7) into Eqs. (2), (6) and the boundary conditions, we obtain the following ODEs, meanwhile the continuity equation is well-satisfied,

$$\frac{\mu_{nf}/\mu_f}{\rho_{nf}/\rho_f} f''' + ff'' = 0 \tag{9}$$

$$\frac{1}{\Pr}\frac{1}{\left(\rho C_p\right)_{nf}/\left(\rho C_p\right)_f}\left(\frac{k_{nf}}{k_f}+\frac{4}{3}Rd\right)\theta''+f\theta'=0 \tag{10}$$

along with the boundary conditions

$$\begin{aligned} &f(0)=S,\ f'(0)=\lambda,\\ &-\tfrac{k_{nf}}{k_f}\theta'(0)=Bi[1-\theta(0)],\\ &f'(\infty)\to 1,\ \theta(\infty)\to 0. \end{aligned} \tag{11}$$

Here, the dimensionless parameters are: Pr is Prandtl number, Rd is the radiation parameter, and Bi is Biot number, which are defined as

$$\Pr=\frac{\nu_f\left(\rho C_p\right)_f}{k_f},\ Rd=\frac{4\sigma^* T_\infty^3}{k^* k_f},\ Bi=\frac{a}{k_f}\sqrt{\frac{\nu_f}{U}}. \tag{12}$$

It is important to state that, we notice Eq. (9) reduces to Eq. (4) from Weidman et al. [8], when $\phi_1=\phi_2=0$ (classical viscous fluid), whilst Eq. (10) was not been considered.

The skin friction coefficient C_f and the local Nusselt number Nu_x are the physical quantities of importance in this study, which are written as

$$\begin{aligned} C_f&=\frac{\mu_{nf}}{\rho_f U^2}\left(\frac{\partial u}{\partial y}\right)_{y=0},\\ Nu_x&=\frac{x}{k_f\left(T_f-T_\infty\right)}\left[-k_{nf}\left(\frac{\partial T}{\partial y}\right)_{y=0}+(q_r)_{y=0}\right]. \end{aligned} \tag{13}$$

After adapting Eq. (7), we can reformulate the physical quantities as

$$\begin{aligned} \sqrt{2}\mathrm{Re}^{1/2}C_f&=\tfrac{\mu_{nf}}{\mu_f}f''(0),\\ \sqrt{2}\mathrm{Re}^{-1/2}Nu_x&=-\left(\tfrac{k_{nf}}{k_f}+\tfrac{4}{3}Rd\right)\theta'(0) \end{aligned} \tag{14}$$

where $\mathrm{Re}=Ux/\nu_f$ is the local Reynolds number.

3 Stability Analysis

Historically, this analysis was performed by Merkin [35] to indicate the stability feature carried by the solution, whether it is stable or non-stable. Since this study produces two solutions, therefore it is required to finalize the investigation by analyzing the stability of the numerical solutions. The procedure begins by modifying Eqs. (2) and (6) to be in the form of a time-dependent version with the unsteady variable, such that

$$\frac{\partial u}{\partial t}+u\frac{\partial u}{\partial x}+v\frac{\partial u}{\partial y}=\frac{\mu_{nf}}{\rho_{nf}}\frac{\partial^2 u}{\partial y^2}, \tag{15}$$

$$\begin{aligned} &\tfrac{\partial T}{\partial t}+u\tfrac{\partial T}{\partial x}+v\tfrac{\partial T}{\partial y}\\ &=\frac{1}{\left(\rho C_p\right)_{nf}}\left(k_{nf}+\tfrac{16\sigma^* T_\infty^3}{3k^*}\right)\tfrac{\partial^2 T}{\partial y^2}. \end{aligned} \tag{16}$$

Then, a new similarity transformation dependable to time is introduced and applied,

$$\begin{aligned} u &= U\frac{\partial f}{\partial \eta}(\eta,\tau),\\ v &= -\left(\frac{Uv_f}{2x}\right)^{1/2}\left[f(\eta,\tau)-\eta\frac{\partial f}{\partial \eta}(\eta,\tau)\right],\\ \theta(\eta,\tau) &= \frac{T-T_\infty}{T_f-T_\infty},\ \eta = y\sqrt{\frac{U}{2xv_f}},\ \tau = Ut/2x \end{aligned} \tag{17}$$

so that Eqs. (15) and (16) become,

$$\frac{\mu_{nf}/\mu_f}{\rho_{nf}/\rho_f}\left(\frac{\partial^3 f}{\partial \eta^3}\right)+f\left(\frac{\partial^2 f}{\partial \eta^2}\right)-\left(\frac{\partial^2 f}{\partial \eta \partial \tau}\right)=0 \tag{18}$$

$$\begin{aligned} &\frac{1}{\Pr}\frac{1}{(\rho C_p)_{nf}/(\rho C_p)_f}\left(\frac{k_{nf}}{k_f}+\frac{4}{3}Rd\right)\frac{\partial^2\theta}{\partial \eta^2}\\ &+f\frac{\partial \theta}{\partial \eta}-\frac{\partial \theta}{\partial \tau}=0 \end{aligned} \tag{19}$$

with the boundary condition

$$\begin{aligned} &f(0,\tau)=S,\ \frac{\partial f}{\partial \eta}(0,\tau)=\lambda,\\ &-\frac{k_{nf}}{k_f}\frac{\partial \theta}{\partial \eta}(0,\tau)=Bi[1-\theta(0,\tau)],\\ &\frac{\partial f}{\partial \eta}(\infty,\tau)\to 1,\ \theta(\infty,\tau)\to 0, \end{aligned} \tag{20}$$

After that, according to Weidman et al. [8], the subsequent perturbation method is adopted

$$\begin{aligned} f(\eta,\tau) &= f_0(\eta)+e^{-\gamma\tau}F(\eta)\\ \theta(\eta,\tau) &= \theta_0(\eta)+e^{-\gamma\tau}G(\eta) \end{aligned} \tag{21}$$

Hence, upon the method adoption with some simplification, and setting $\tau = 0$, the eigenvalue equations are

$$\frac{\mu_{nf}/\mu_f}{\rho_{nf}/\rho_f}F'''+\left(f_0F''+Ff_0''\right)+\gamma F'=0 \tag{22}$$

$$\begin{aligned} &\frac{1}{\Pr}\frac{1}{(\rho C_p)_{nf}/(\rho C_p)_f}\left(\frac{k_{nf}}{k_f}+\frac{4}{3}Rd\right)G''\\ &+\left(f_0G'+F\theta_0'\right)+\gamma G=0 \end{aligned} \tag{23}$$

respect to the boundary condition:

$$\begin{aligned} &F(0)=0,\ F'(0)=0,\ \frac{k_{nf}}{k_f}G'(0)=BiG(0)\\ &F'(\infty)\to 0,\ G(\infty)\to 0 \end{aligned} \tag{24}$$

To generate the possible eigenvalues, Harris et al. [36] suggested any suitable conditions as $\eta \to \infty$ to be relaxed (i.e. $F'(\infty)\to 0$) and a new condition (i.e. $F''(0)=1$) is inserted. By implementing the suggestion and solving Eqs. (22)–(24) with the facilitation of bvp4c, an infinite eigenvalue is generated $\gamma_1 < \gamma_2 < \gamma_3 ...$ Where the solution is said to be real only when $\gamma_1 > 0$.

4 Results and Discussion

Before generating the new results from the present model, we need to verify the numerical computation. Comparison has been made with the previously published findings by Khashi'ie et al. [46], Zainal et al. [47], Mohd Rohni et al. [48], and Weidman et al. [8] for certain limiting cases as displayed in Tables 3 and 4. The outcomes are remarkable in agreement with the published findings, which also means that the model and the computation in the present solver scheme are well formulated and computed. We also provide the data tabulation for the present flow model for future reference in Tables 5 and 6 for the skin friction coefficient and the local Nusselt number for selected λ of the magnetic nanofluids.

The numerical outcomes for the present model are articulated graphically as displayed in Figs. 2, 3, 4, 5, 6 and 7. The Prandtl number is designed to stay constant throughout this investigation with the amount of $\mathrm{Pr} = 6.96$ referencing to the base liquid (water). The following range is established for the other parameters to provide the possible outcome; $-0.5 \leq S \leq 0.5$, $1 \leq Rd \leq 10$, $1 \leq Bi \leq 10$, $-1 < \lambda \leq 2$. In most of these figures, it should be observable that there are two possible outcomes are generated. It is also seen that the second solution only appears at the negative region of λ, which is when the plate is moving towards the slit. Hence, this also implies that the second solution is only possible to be generated if we apply the negative value towards the moving plate parameter ($\lambda < 0$), or otherwise, we cannot attain the dual solution. However, even there are two possible outcomes are generated, we can only rely on one of them and neglect the alternative outcome due to the non-stable feature.

Figures 2 and 3 portray the distribution of $\sqrt{2}\mathrm{Re}^{1/2}C_f$ and $\sqrt{2}\mathrm{Re}^{-1/2}Nu_x$ against the moving parameter of the plate for two different water-based MNFs which are cobalt ferrite nanofluid and Mn-Zn ferrite nanofluid. The volume fraction for the MNP is specified to be $\phi = 1\%$ for each type of MNFs, meanwhile, the other parameters are specified as follows: $S = 0.5$, $Bi = Rd = 1$. Under these specified conditions, for the first solution, cobalt ferrite MNF has a moderately greater $\sqrt{2}\mathrm{Re}^{1/2}C_f$ and $\sqrt{2}\mathrm{Re}^{-1/2}Nu_x$

Table 3. Comparison values for $f''(0)$ at the selected λ when $S = 0$ for copper-water nanofluid with $\phi = 0.1$

λ	First solution			Second solution		
	Present	Khashi'ie et al. [46] & Zainal et al. [47]	Mohd Rohni et al. [48]	Present	Khashi'ie et al. [46] & Zainal et al. [47]	Mohd Rohni et al. [48]
−0.2000	0.505317779	0.505318	0.5053	0.026061434	0.026061	0.0261
−0.2500	0.471688345	0.471688	0.4717	0.053322207	0.053322	0.0533
−0.3000	0.418959116	0.418959	0.4190	0.099701700	0.099702	0.0997
−0.3500	0.302592535	0.302592	0.3028	0.209760590	0.209761	0.2097
−0.3541	0.257961808	0.257961	0.2623	0.253876406	0.253877	–

Table 4. Comparison values for γ_1 at the selected S and λ when $\phi = Rd = 0$ in the absence of convective boundary condition

S	λ	Smallest eigenvalues $\gamma_1\gamma_1$			
		First solution		Second solution	
		Present	Weidman et al. [8]	Present	Weidman et al. [8]
0.00	0.00	0.8096	0.8096	–	–
	−0.30	0.2470	0.2470	−0.1332	−0.1332
	−0.35	0.0577	0.0576	−0.0492	−0.0492
−0.25	0.00	0.5524	0.5524	–	–
	−0.200	0.1045	0.1045	−0.0701	−0.0701
	−0.212	0.0403	0.0403	−0.0341	−0.0341
0.25	0.00	1.0852	1.0852	–	–
	−0.500	0.1588	0.1588	−0.1158	−0.1158
	−0.520	0.0473	0.0473	−0.0428	−0.0428

Table 5. Values of $\sqrt{2}\mathrm{Re}^{1/2}C_f$ at the selected λ when $Bi = Rd = 1, S = 0.5$ for cobalt-ferrite nanofluid and Mn-Zn ferrite nanofluid with $\phi = 0.01$

λ	First solution		Second solution	
	Cobalt ferrite/water	Mn-Zn ferrite/water	Cobalt ferrite/water	Mn-Zn ferrite/water
−0.60	0.926288516	0.926223395	0.280704347	0.280701259
−0.65	0.874575405	0.874505184	0.359348206	0.359348229
−0.70	0.780082225	0.779993447	0.480813606	0.480830197

Table 6. Values of $\sqrt{2}\mathrm{Re}^{-1/2}Nu_x$ at the selected λ when $Bi = Rd = 1, S = 0.5$ for cobalt-ferrite nanofluid and Mn-Zn ferrite nanofluid with $\phi = 0.01$

λ	First solution		Second solution	
	Cobalt ferrite-water	Mn-Zn ferrite-water	Cobalt ferrite-water	Mn-Zn ferrite-water
−0.60	1.254023586	1.253760150	0.327589760	0.327797638
−0.65	1.195216646	1.195031290	0.485409845	0.485686416
−0.70	1.093215342	1.093133116	0.702984236	0.703290237

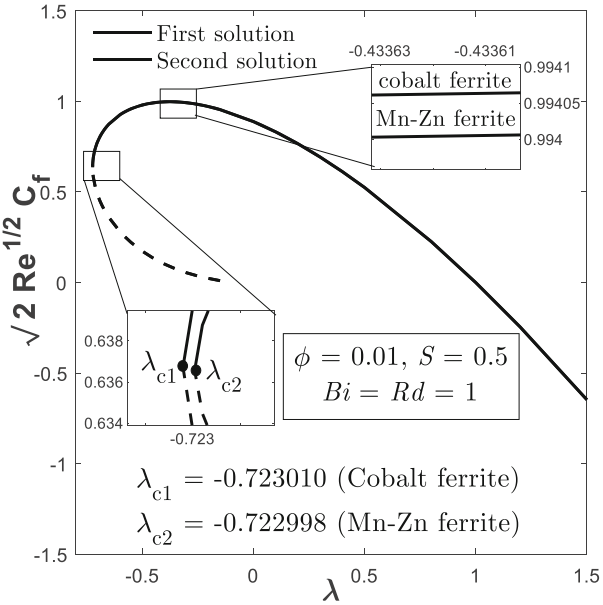

Fig. 2. Skin friction coefficient against λ for different MNFs

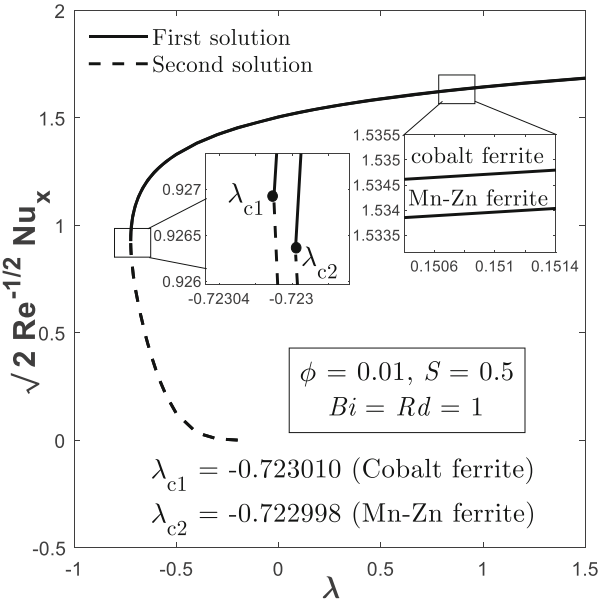

Fig. 3. Local Nusselt number against λ for different MNFs

than Mn-Zn ferrite MNF. The boundary layer separation for these MNFs occurred at the negative region of the moving plate parameter which is at $\lambda_c = -0.72301$ for cobalt ferrite MNF and $\lambda_c = -0.722998$ for Mn-Zn ferrite MNF. Although the critical point for these two MNFs is quite near and not that different, we still can deduce that cobalt ferrite MNF is preferable in preventing the boundary layer separation compared to the other one.

In Figs. 2 and 3 too, the first solution of $\sqrt{2}\mathrm{Re}^{1/2}C_f$ is contemplated to be rapidly increasing when the moving plate parameter goes from the positive region to the negative region. Approximately, the highest value of $\sqrt{2}\mathrm{Re}^{1/2}C_f$ is achieved when $\lambda \approx -0.4$ and after this value, $\sqrt{2}\mathrm{Re}^{1/2}C_f$ starts to decrease before reaching the critical point that declares the separation of the boundary layer. However, the adverse impact is noticed for the first solution of $\sqrt{2}\mathrm{Re}^{-1/2}Nu_x$. The heat transfer rate for MNFs is predicted to increase when the plate is moving out from the slit which is when the value of the moving plate parameter increase.

Figures 4 and 5 unveil the impact of thermal radiation parameter and Biot number towards $\sqrt{2}\mathrm{Re}^{-1/2}Nu_x$, respectively, against the moving plate parameter specifically for cobalt ferrite MNF when $\phi = 0.01$, $S = 0.5$. The thermal radiation parameter and Biot number are contemplated to simulate the same behavior towards $\sqrt{2}\mathrm{Re}^{-1/2}Nu_x$. The boost in these parameters enable $\sqrt{2}\mathrm{Re}^{-1/2}Nu_x$ for the first solution to be enhanced without affecting the boundary layer separation. In other words, the boundary layer separation point remains the same at $\lambda_c = -0.72301$ although we choose a different value for the thermal radiation parameter and Biot number.

Furthermore, Figs. 6 and 7 expose the impact of suction parameter towards the distribution of $\sqrt{2}\mathrm{Re}^{1/2}C_f$ and $\sqrt{2}\mathrm{Re}^{-1/2}Nu_x$ against the moving plate parameter, respectively, for cobalt ferrite MNF when $\phi = 0.01$, $Rd = Bi = 1$. As we focus on the first solution, the escalation of the suction parameter is observed to diminish $\sqrt{2}\mathrm{Re}^{1/2}C_f$ at

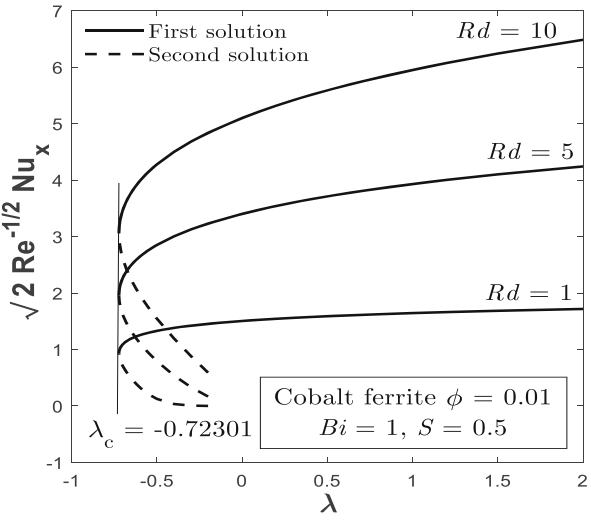

Fig. 4. Local Nusselt number against λ for different radiation parameter

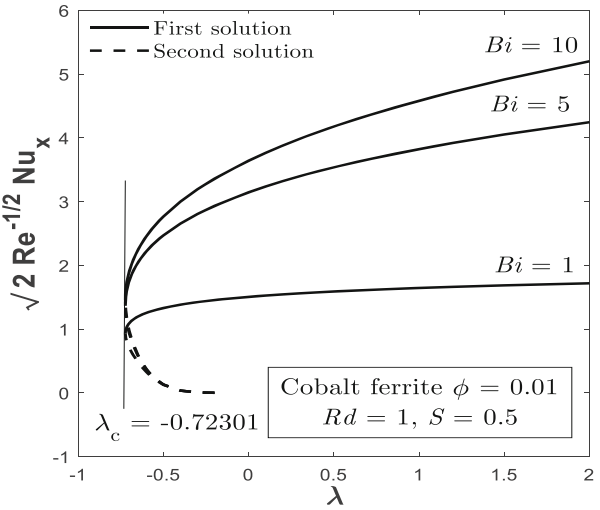

Fig. 5. Local Nusselt number against λ for different Biot number

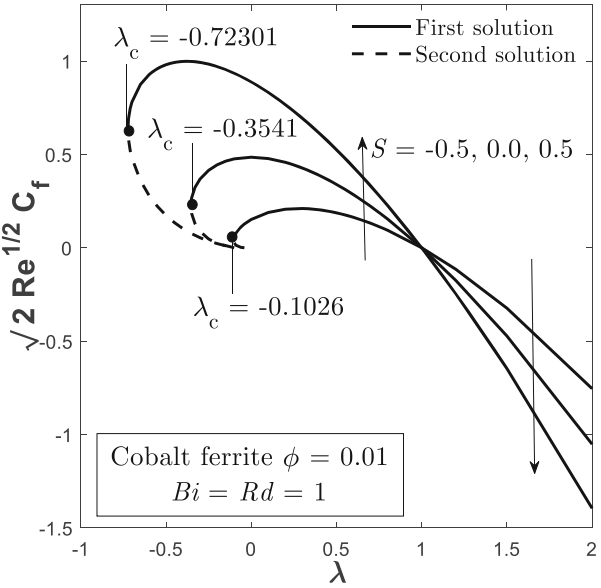

Fig. 6. Skin friction coefficient agains λ for different suction parameter

the region when $1 < \lambda \leq 2$, meanwhile the reverse effect has occurred at the region when $\lambda_c \leq \lambda < 1$. Physically, the boost in suction may aid in the migration of the fluid particles towards the wall. When the plate is moving in an opposite direction from the fluid, this causes the velocity gradient at the surface to increase and improves the skin

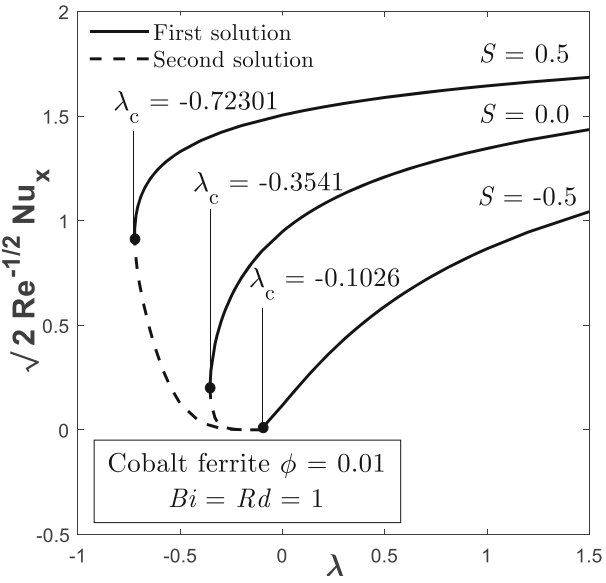

Fig. 7. Local Nusselt number against λ for different suction parameter

friction. The point of $(1, 0)$ is noted to be the focal point that conflicts the behavior of the suction parameter towards $\sqrt{2}\mathrm{Re}^{1/2}C_f$, which also pointed.

out zero-skin friction happens when $\lambda = 1$ as the free stream of the fluid is equally moving with the same velocity as the plate [46]. Moreover, in the aspect of the heat transfer, the strengthening in this parameter has amplified the $\sqrt{2}\mathrm{Re}^{-1/2}Nu_x$ efficiently for the first solution, especially when a higher value of λ is applied. The boundary layer separation point for these figures too (see Figs. 6 and 7) is seen to be projected at the negative region of λ which is at, $\lambda_c = -0.10260, -0.35410, -0.72301$ for $S = -0.5, 0.0, 0.5$, respectively. This kind of occurrence also signifies that the boundary layer separation can be prevented if a higher suction parameter is imposed.

As previously discussed, there are two possible outcomes are observed to be generated from this flow model. But for sure, only one outcome can be used for the actual application. In most of the cases observed before, we can perceive that the first solution is the most realizable one. Anyhow, this initial assumption needs to be validated through a stability analysis. According to our findings from the analysis, the first solution is real as it is more stable than the other one. In Fig. 8, we have illustrated the distribution of the smallest eigenvalues γ_1 against the moving plate parameter when $S = 0.5$, $Bi = Rd = 1$ and $\phi = 0.01$ for cobalt ferrite MNF. It is validated from Fig. 8 that the first solution is the practical predicted solution as it provides the positive smallest eigenvalue that signifies the stable property carried by the solution when the perturbation equations are implied. However, the second solution gives the negative smallest eigenvalue due to the growth of perturbation that implies the non-stable property, which is not realizable for practical use. Therefore, only the first solution can be relied upon for prediction in actual application.

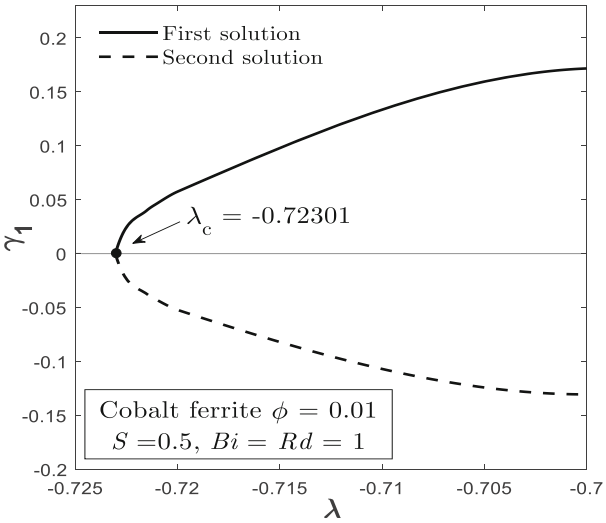

Fig. 8. Distribution of the smallest eigenvalues

5 Conclusion

The mathematical model for the boundary layer flow and heat transfer of MNFs over a moving surface with convective boundary condition and radiation effects are successfully formulated and solved. Two types of water-based MNFs are chosen, which are the cobalt ferrite MNF and Mn-Zn ferrite MNF. The MNF containing cobalt ferrite is deduced to have better heat transfer properties and skin friction rate compared to the other one. Two possible numerical outcomes can be generated within the specific value of controlling parameters, but only the first solution can be relied on for practical usage. Therefore, from the first solution, we can draw the following conclusions:

- The heat transfer performance is much more effective when a suitable larger value of Biot number, thermal radiation, suction, and moving plate parameter is applied.
- The boundary layer separation can be prevented by using a stronger suction effect; meanwhile, the thermal radiation and Biot number cannot be used in controlling the separation.
- The skin friction coefficient is larger when the plate is moving towards the slit, especially when the suction parameter is enlarging.

This study is significant in giving an initial simulation for the behavior of MNFs and provides insight into controlling the specified parameter to achieve the desired output, especially for cooling/heating activities. However, the findings in this study are only confidently reliable for the application that is within the specified model description and geometry.

Acknowledgments. The authors gladly appreciate the support from the following organizations: Ministry of Higher Education Malaysia (MOHE) for the Fundamental Research Grant Scheme (KPTFRGS/1/2019/STG06/IPM/02/3, Vot 5540309), Universiti Putra Malaysia, and Universiti Teknikal Malaysia Melaka.

References

1. Moutsoglou, A., Bhattacharya, A.K.: Laminar and turbulent boundary layers on moving, nonisothermal continuous flat surfaces. J. Heat Transfer **104**(4), 707–714 (1982). https://doi.org/10.1115/1.3245189
2. Das, K.: Radiation and melting effects on MHD boundary layer flow over a moving surface. Ain Shams Eng. J. **5**(4), 1207–1214 (2014). https://doi.org/10.1016/j.asej.2014.04.008
3. Sakiadis, B.C.: Boundary-layer behavior on continuous solid surfaces: I. Boundary-layer equations for two-dimensional and axisymmetric flow. AIChE J. **7**(1), 26–28 (1961). https://doi.org/10.1002/aic.690070108
4. Sakiadis, B.C.: Boundary-layer behavior on continuous solid surfaces: II. The boundary layer on a continuous flat surface. AIChE J. **7**(2), 221–225 (1961). https://doi.org/10.1002/aic.690070211
5. Chappidi, P.R., Gunnerson, F.S.: Analysis of heat and momentum transport along a moving surface. Int. J. Heat Mass Transf. **32**(7), 1383–1386 (1989). https://doi.org/10.1016/0017-9310(89)90039-2
6. Afzal, N.: Turbulent boundary layer on a moving continous plate. Fluid Dyn. Res. **17**(4), 181–194 (1996). https://doi.org/10.1016/0169-5983(95)00032-1
7. Howell, T.G., Jeng, D.R., De Witt, K.J.: Momentum and heat transfer on a continuous moving surface in a power law fluid. Int. J. Heat Mass Transf. **40**(8), 1853–1861 (1997). https://doi.org/10.1016/S0017-9310(96)00247-5
8. Weidman, P.D., Kubitschek, D.G., Davis, A.M.J.: The effect of transpiration on self-similar boundary layer flow over moving surfaces. Int. J. Eng. Sci. **44**(11–12), 730–737 (2006). https://doi.org/10.1016/j.ijengsci.2006.04.005
9. Ishak, A., Nazar, R., Bachok, N., Pop, I.: Melting heat transfer in steady laminar flow over a moving surface. Heat Mass Transf. **46**(4), 463–468 (2010). https://doi.org/10.1007/s00231-010-0592-8
10. Subhashini, S.V., Sumathi, R.: Dual solutions of a mixed convection flow of nanofluids over a moving vertical plate. Int. J. Heat Mass Transf. **71**, 117–124 (2014). https://doi.org/10.1016/j.ijheatmasstransfer.2013.12.034
11. Das, S., Jana, R.N.: Natural convective magneto-nanofluid flow and radiative heat transfer past a moving vertical plate. Alex. Eng. J. **54**(1), 55–64 (2015). https://doi.org/10.1016/j.aej.2015.01.001
12. Aladdin, N.A.L., Bachok, N., Pop, I.: Cu-Al_2O_3/water hybrid nanofluid flow over a permeable moving surface in presence of hydromagnetic and suction effects. Alex. Eng. J. **59**(2), 657–666 (2020). https://doi.org/10.1016/j.aej.2020.01.028
13. Waini, I., Ishak, A., Pop, I.: Flow and heat transfer of a hybrid nanofluid past a permeable moving surface. Chin. J. Phys. **66**, 606–619 (2020). https://doi.org/10.1016/j.cjph.2020.04.024
14. Khashi'ie, N.S., Md Arifin, N., Pop, I., Nazar, R.: Melting heat transfer in hybrid nanofluid flow along a moving surface. J. Therm. Anal. Calorim. **147**(1), 567–578 (2020). https://doi.org/10.1007/s10973-020-10238-4

15. Anuar, N.S., Bachok, N., Arifin, N.M., Rosali, H.: Role of multiple solutions in flow of nanofluids with carbon nanotubes over a vertical permeable moving plate. Alex. Eng. J. **59**(2), 763–773 (2020). https://doi.org/10.1016/j.aej.2020.02.015
16. Hussein, A.M., Sharma, K.V., Bakar, R.A., Kadirgama, K.: A review of forced convection heat transfer enhancement and hydrodynamic characteristics of a nanofluid. Renew. Sustain. Energy Rev. **29**, 734–743 (2014). https://doi.org/10.1016/j.rser.2013.08.014
17. Moita, A., Moreira, A., Pereira, J.: Nanofluids for the next generation thermal management of electronics: a review. Symmetry **13**(8), 1362 (2021). https://doi.org/10.3390/sym13081362
18. Genc, S., Derin, B.: Synthesis and rheology of ferrofluids: a review. Curr. Opin. Chem. Eng. **3**, 118–124 (2014). https://doi.org/10.1016/j.coche.2013.12.006
19. Odenbach, S.: Recent progress in magnetic fluid research. J. Phys. Condens. Matter. **16**(32), R1135–R1150 (2004). https://doi.org/10.1088/0953-8984/16/32/R02
20. Khan, W.A., Khan, Z.H., Haq, R.U.: Flow and heat transfer of ferrofluids over a flat plate with uniform heat flux. Eur. Phys. J. Plus **130**(4), 86 (2015). https://doi.org/10.1140/epjp/i2015-15086-4
21. Raj, K., Moskowitz, R.: Commercial applications of ferrofluids. J. Magn. Magn. Mater. **85**(1–3), 233–245 (1990). https://doi.org/10.1016/0304-8853(90)90058-X
22. Marszałł, M.P.: Application of magnetic nanoparticles in pharmaceutical sciences. Pharm Res. **28**(3), 480–483 (2011). https://doi.org/10.1007/s11095-010-0284-6
23. Kumar, A., Subudhi, S.: Preparation, characteristics, convection and applications of magnetic nanofluids: a review. Heat Mass Transf. **54**(2), 241–265 (2017). https://doi.org/10.1007/s00231-017-2114-4
24. Kole, M., Khandekar, S.: Engineering applications of ferrofluids: a review. J. Magn. Magn. Mater. **537**, 168222 (2021). https://doi.org/10.1016/j.jmmm.2021.168222
25. Rashad, A.M.: Impact of anisotropic slip on transient three dimensional MHD flow of ferrofluid over an inclined radiate stretching surface. J. Egypt. Math. Soc. **25**(2), 230–237 (2017). https://doi.org/10.1016/j.joems.2016.12.001
26. Kumar, P.B.S., Gireesha, B.J., Mahanthesh, B., Gorla, R.S.R.: Radiative nonlinear 3D flow of ferrofluid with Joule heating, convective condition and Coriolis force. Thermal Sci. Eng. Progr. **3**, 88–94 (2017). https://doi.org/10.1016/j.tsep.2017.06.006
27. Hassan, M., Fetecau, C., Majeed, A., Zeeshan, A.: Effects of iron nanoparticles' shape on convective flow of ferrofluid under highly oscillating magnetic field over stretchable rotating disk. J. Magn. Magn. Mater. **465**, 531–539 (2018). https://doi.org/10.1016/j.jmmm.2018.06.019
28. Shafii, M.B., Keshavarz, M.: Experimental study of internal forced convection of ferrofluid flow in non-magnetizable/magnetizable porous media. Exp. Thermal Fluid Sci. **96**, 441–450 (2018). https://doi.org/10.1016/j.expthermflusci.2018.03.036
29. Özdemir, M.R., et al.: Experimental studies on ferrofluid pool boiling in the presence of external magnetic force. Appl. Therm. Eng. **139**, 598–608 (2018). https://doi.org/10.1016/j.applthermaleng.2018.05.013
30. Zhang, X., Zhang, Y.: Experimental study on enhanced heat transfer and flow performance of magnetic nanofluids under alternating magnetic field. Int. J. Therm. Sci. **164**, 106897 (2021). https://doi.org/10.1016/j.ijthermalsci.2021.106897
31. Lee, A., Jeon, Y., Chinnasamy, V., Cho, H.: Investigation of forced convective heat transfer with magnetic field effect on water/ethylene glycol-cobalt zinc ferrite nanofluid. Int. Commun. Heat Mass Transfer **128**, 105647 (2021). https://doi.org/10.1016/j.icheatmasstransfer.2021.105647
32. Wahid, N.S., Arifin, N.M., Khashi'ie, N.S., Pop, I.: Hybrid nanofluid slip flow over an exponentially stretching/shrinking permeable sheet with heat generation. Mathematics **9**(1), 30 (2021). https://doi.org/10.3390/math9010030

33. Wahid, N.S., Arifin, N.M., Khashi'ie, N.S., Pop, I., Bachok, N., Hafidzuddin, M.E.H.: Mixed convection magnetic nanofluid flow past a rotating vertical porous cone. JAFM **15**(4), 1207–1220 (2022). https://doi.org/10.47176/jafm.15.04.1063
34. Ho, C.J., Liu, W.K., Chang, Y.S., Lin, C.C.: Natural convection heat transfer of alumina-water nanofluid in vertical square enclosures: an experimental study. Int. J. Therm. Sci. **49**(8), 1345–1353 (2010). https://doi.org/10.1016/j.ijthermalsci.2010.02.013
35. Merkin, J.H.: On dual solutions occurring in mixed convection in a porous medium. J Eng. Math. **20**(2), 171–179 (1986). https://doi.org/10.1007/BF00042775
36. Harris, S.D., Ingham, D.B., Pop, I.: Mixed Convection boundary-layer flow near the stagnation point on a vertical surface in a porous medium: brinkman model with slip. Transp. Porous Med. **77**(2), 267–285 (2009). https://doi.org/10.1007/s11242-008-9309-6
37. Kameswaran, P.K., Sibanda, P., Murti, A.S.N.: Nanofluid flow over a permeable surface with convective boundary conditions and radiative heat transfer. Math. Probl. Eng. **2013**, 1–11 . https://doi.org/10.1155/2013/201219
38. Sheremet, M.A., Pop, I., Rosca, A.V.: The influence of thermal radiation on unsteady free convection in inclined enclosures filled by a nanofluid with sinusoidal boundary conditions. HFF **28**(8), 1738–1753 (2018). https://doi.org/10.1108/HFF-09-2017-0375
39. Ahmed, N., et al.: Applications of nanofluids for the thermal enhancement in radiative and dissipative flow over a wedge. Appl. Sci. **9**(10), 1976 (2019). https://doi.org/10.3390/app9101976
40. Rosseland, S.: Astrophysik auf atomtheoretischer Grundlage. J. Springer, Berlin (1931)
41. Cortell Bataller, R.: Radiation effects in the Blasius flow. Appl. Math. Comput. **198**(1), 333–338 (2008). https://doi.org/10.1016/j.amc.2007.08.037
42. Cortell, R.: Effects of viscous dissipation and radiation on the thermal boundary layer over a nonlinearly stretching sheet. Phys. Lett. A **372**(5), 631–636 (2008). https://doi.org/10.1016/j.physleta.2007.08.005
43. Ishak, A.: Thermal boundary layer flow over a stretching sheet in a micropolar fluid with radiation effect. Meccanica **45**(3), 367–373 (2010). https://doi.org/10.1007/s11012-009-9257-4
44. Ishak, A., Yacob, N.A., Bachok, N.: Radiation effects on the thermal boundary layer flow over a moving plate with convective boundary condition. Meccanica **46**(4), 795–801 (2011). https://doi.org/10.1007/s11012-010-9338-4
45. Magyari, E., Pantokratoras, A.: Note on the effect of thermal radiation in the linearized Rosseland approximation on the heat transfer characteristics of various boundary layer flows. Int. Commun. Heat Mass Transf. **38**(5), 554–556 (2011). https://doi.org/10.1016/j.icheatmasstransfer.2011.03.006
46. Khashi'ie, N.S., Arifin, N.M., Pop, I.: Magnetohydrodynamics (MHD) boundary layer flow of hybrid nanofluid over a moving plate with Joule heating. Alexandria Eng. J. **61**(3), 1938–1945 (2022). https://doi.org/10.1016/j.aej.2021.07.032
47. Zainal, N.A., Nazar, R., Naganthran, K., Pop, I.: MHD flow and heat transfer of hybrid nanofluid over a permeable moving surface in the presence of thermal radiation. HFF **31**(3), 858–879 (2021). https://doi.org/10.1108/HFF-03-2020-0126
48. Rohni, A.M., Ahmad, S., Pop, I.: Boundary layer flow over a moving surface in a nanofluid beneath a uniform free stream. Int. J. Numer. Meth. HFF **21**(7), 828–846 (2011). https://doi.org/10.1108/09615531111162819